ADVANCED FUNCTIONAL MATERIALS
www.afm-journal.de

A Highly Sensitive Surface Electrode for Electrophysiological Monitoring

*Jiang Lu, Qianming Li, Qingyun Huang, Dan Li, Yiding Jiao, Yuanzhen Wang, Yiran Li, Kuangyi Zou, Zilin Chen, Jiayi Gu, Hanting Zhang, Jiacheng Wang, Fangyan Li, Shuo Yang, Tingting Ye, Jie Song, Er He, and Ye Zhang**

Surface electrodes monitoring various electrophysiological activities with high sensitivity are crucial for studying electrical phenomena in living organisms. However, the sensitivity of current surface electrodes is limited due to electron transmission losses and signal attenuation at the electrode-skin interface. Here, a bicontinuous liquid metal/polymer film electrode is developed, in which up to 92 wt.% of liquid metal is stably immobilized within a 3D continuous polymer network via electrostatic interactions. This electrode facilitates fast electron transport, enhances skin adhesion through hydrogen bonding, and ensures conformal contact due to its flexibility. As a result, the electrode achieves a sensitivity of 20 μV N^{-1}, representing an improvement of 400% over the highest performance reported to date. This leap in sensitivity enables the high-resolution monitoring of electrophysiological signals, allowing for earlier and more accurate identification of myocardial infarction abnormalities. Moreover, this high-sensitivity electrode has the potential to develop an intelligent sensory system for material recognition and provide real-time warnings in hazardous situations for individuals with tactile impairments.

1. Introduction

Electrophysiological signals are generated by the electrical activities within an organism, capable of providing abundant physiological and pathological information.[1–5] Surface electrodes are commonly used to monitor these signals, and even slight changes reflect complex biological activities.[6–8] Monitoring these slight changes is crucial for the early detection of certain potential micro-lesions (such as arrhythmias, an early sign of myocardial infarction),[9,10] as early detection can greatly reduce the risk of severe complications.[11–13] Therefore, high-sensitivity surface electrodes capable of accurately monitoring these slight changes are crucial for medical diagnostics and health management.[14,15]

However, due to electronic transmission losses and signal attenuation at the electrode-skin interface,[16–18] fabricating high-sensitivity surface electrodes using existing electrode materials remains challenging.[19,20] As be deduced from the schematic illustration of the electrode's work on the skin surface and its simplified equivalent circuit model (**Figure 1a**, the details of the model are shown in the Supporting Information), to achieve high sensitivity, the electrode material should possess high conductivity and low interfacial impedance. Metal electrodes typically exhibit high conductivity but struggle to establish a stable electrode-skin interface, resulting in high interfacial impedance.[21] Conductive polymer electrodes[22,1] (such as polypyrrole and polyaniline) and conductive composite electrodes[23–25] can form better interfaces with the skin, but their limited conductivity leads to signal loss. To the best of our knowledge, the maximum sensitivity of currently reported surface electrodes is only 5 μV N^{-1}, which is still insufficient for monitoring slight characteristic signal changes.[26] Therefore, high-sensitivity surface electrodes remain an urgent need.

Here, we have developed a bicontinuous liquid metal/polymer film electrode, in which up to 92 wt.% of liquid metal was stably immobilized within a 3D continuous polymer network via electrostatic interactions. The liquid metal formed a continuous conductive path, effectively minimizing electronic

J. Lu, Q. Li, Y. Jiao, Y. Wang, Y. Li, K. Zou, Z. Chen, J. Gu, H. Zhang, J. Wang, F. Li, S. Yang, T. Ye, J. Song, E. He, Y. Zhang
College of Engineering and Applied Sciences
National Laboratory of Solid State Microstructures
Jiangsu Key Laboratory of Artificial Functional Materials
Chemistry and Biomedicine Innovation Centre
Collaborative Innovation Centre of Advanced Microstructures
Nanjing University
Nanjing 210023, China
E-mail: yezhang@nju.edu.cn

Q. Huang
State Key Laboratory of Systems Medicine for Cancer
Center for Single-Cell Omics
School of Public Health
Shanghai Jiao Tong University School of Medicine
Shanghai 200025, China

D. Li
Key Laboratory of Inflammation and Immunoregulation
School of Medicine and Holistic Integrative Medicine
Nanjing University of Chinese Medicine
Nanjing 210023, China

The ORCID identification number(s) for the author(s) of this article can be found under https://doi.org/10.1002/adfm.202421132

DOI: 10.1002/adfm.202421132

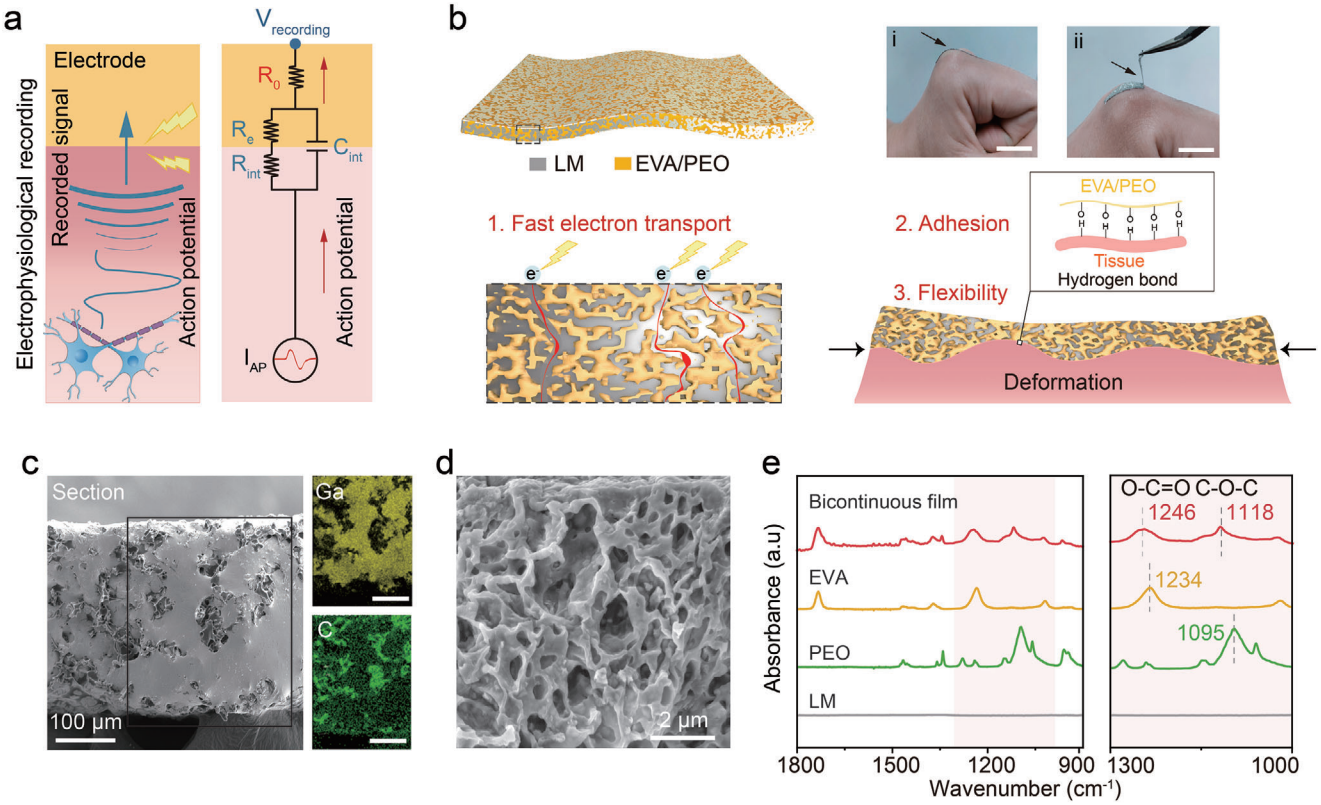

Figure 1. Schematic illustration and structural characterizations of the bicontinuous film. a) Functional mode of electrophysiological recording between humans and bicontinuous film electrodes. R_{int}, the resistance of the bicontinuous film interface; R_0, the interconnect resistance of the bicontinuous film; C_{int}, the capacitance of the bicontinuous film interface; R_e, bicontinuous film resistance; $V_{recording}$, the electric potential of the electrophysiological recording. b) Schematic illustration of the bicontinuous film for electrophysiological recording and optical images for (i) conformal contacting and (ii) adhering to the skin. c) Cross-sectional scanning electron microscopy (SEM) image and corresponding energy-dispersive spectroscopy (EDS) elemental mappings of the bicontinuous film. d) SEM image of the polymer network obtained by etching the liquid metal in the bicontinuous film with HCl. e) Fourier-transform infrared spectroscopy (FTIR) spectra of liquid metal (LM), poly (ethylene oxide) (PEO), ethylene-vinyl-acetate (EVA), and bicontinuous film.

transmission losses. Hydrogen bonding between the polymer and the skin surface ensured adhesion ability, thereby reducing interfacial impedance. Besides, the electrode also exhibited flexibility to conform to the skin's deformation (Figure 1b). As a result, the electrode achieved a sensitivity of 20 μV N^{-1}, ≈400% higher than the best previously reported performance. The electrode could provide high-sensitivity electrophysiological signals, allowing for earlier detection of abnormal myocardial infarction signals. Furthermore, it can be integrated into intelligent sensory systems for material recognition and provide real-time warnings in hazardous situations for individuals with tactile impairments.

2. Results and Discussion

2.1. Design and Characterization of the Bicontinuous Film

The fabrication process of the bicontinuous film is schematically illustrated in Figure S1 (Supporting Information). Ethylene-vinyl-acetate is an elastomeric polymer but has limited flexibility and adhesion. Poly (ethylene oxide) was mixed well with ethylene-vinyl-acetate solution to form a continuous polymer matrix, enhancing the adhesion and lowering the modulus. Initially, the liquid metal is uniformly dispersed in the polymer solution by vigorous shearing, forming liquid metal-polymer droplets with a core-shell structure (Figure S2I, Supporting Information). The solution was transferred to a culture dish and processed by vacuum drying at 80 °C. Liquid metal droplets were dispersed in the physically crosslinked polymer network which entrapped a substantial amount of solvent (Figure S2II, Supporting Information). As drying continued, the solvent in the networks gradually evaporated (Figure S2III, Supporting Information). Volume shrinkage during drying (Figure S3a, Supporting Information) caused the oxide layer on the surface of the liquid metal to rupture under compressive stress, forming continuous conductive pathways embedded in the polymer network (Figure S2IV, Supporting Information). The conductive pathways are also further evidenced by the sudden transition of the film's resistance from an insulating state to a conductive state in the later stages of drying (Figure S3b, Supporting Information). Finally, the liquid metal infiltrated the polymer networks, forming a continuum in the structure with an average content of 92 wt.% (Figure S4, Supporting Information). In contrast to previous reported thermal sintering methods,[27,28] this work requires a lower temperature for solvent evaporation,

which enables adequate volumetric shrinkage that leads to the rupturing of the oxide layer and promotes the merging of liquid metal droplets. X-ray photoelectron spectroscopy coupled with the Ar etching technique was used to analyze the surface information of the electrode. The outermost layer of the film consisted of polymers (88% vol) and gallium (12% vol). After etching 20 nm, the liquid metal content increased to over 71% vol. As the etching depth increased to 160 nm, the liquid metal content increased to over 90% vol, while the polymer content decreased to below 10% vol (Figure S5, Supporting Information). The cross-sectional scanning electron microscopy image of the film and the continuous distribution of Ga elements proved the continuous structure of the liquid metal (Figure 1c). After etching the liquid metal in the film with hydrochloric acid, a 3D continuous polymer network with uniformly distributed pores was observed (Figure 1d), further verifying the bicontinuous structure of the film.

Fourier-transform infrared spectroscopy exhibited that the absorption peak of the O—C=O bond of the bicontinuous film shifted from 1234 cm^{-1} in pure polymer to 1246 cm^{-1}. Similarly, the absorption peak corresponding to the C—O—C bond shifted from 1095 to 1118 cm^{-1} (Figure 1e). The shifts were attributed to charge redistribution resulting from electrostatic interactions among O—C=O groups on EVA, the C—O—C groups on PEO, and the oxidized liquid metal. The electrostatic interactions were also verified by both the increase in decomposition temperature (Figure S6, Supporting Information) and the linear viscoelastic region prolong of the bicontinuous film (Figure S7, Supporting Information). Electrostatic interactions ensured the immobilization of the high content of liquid metal within the polymer network, forming stable conductive pathways.

2.2. Electrical and Mechanical Performance

The bicontinuous film showed excellent electrical and mechanical properties. The electrical conductivity increased with increasing mass fraction of liquid metal in the film, reaching the highest value of 1.2×10^6 S m^{-1} (**Figure 2a**). The electrical conductivity changed by less than 3% after immersion in simulated sweat for one week (Figure S8, Supporting Information). The film also showed adhesiveness to the skin; as the PEO loading increased, the adhesion force correspondingly increased while the conductivity decreased (Figures S9 and S10, Supporting Information). The bicontinuous film with 2% PEO loading was finally selected. Its thickness was ≈40 µm, exhibiting a fracture strain of 80% that matched that of skin and a high adhesion strength of 45 N m^{-1} (Figure 2b; Figure S11, Supporting Information). The PEO molecular chain contained numerous repeating units (C—O—C), whose oxygen atoms carried lone pairs of electrons and could serve as hydrogen bond acceptors. The skin surface's stratum corneum, keratin, and lipids contained numerous hydrogen bond donors, such as hydroxyl, amino, and carboxyl groups.[26] When the bicontinuous film came into contact with the skin, the oxygen atoms in PEO acted as hydrogen bond acceptors, forming hydrogen bonds with the hydroxyl and amino groups on the skin's surface. This hydrogen bonding effect enhanced the adhesion of the film to the skin surface.[29] The film was reusable, and the corresponding adhesion strength to the skin hardly decreased after 8 cycles of attach/detach (Figure S12, Supporting Information). In addition, the adhesion strength of the film was virtually unaffected by various deformations (Figure 2d) and showed no significant change after adhering to porcine skin for 7 days (Figure S13, Supporting Information). The bicontinuous film also possessed skin-like Young's modulus of only 400 kPa (Figure 2c), which exhibited excellent conformability to the skin and remained mechanically robust after multiple cycles of tensile testing (Figure S14, Supporting Information). Furthermore, the film displayed reliable electromechanical coupling properties under complex deformations including bending, twisting, compression, and friction, over 5000 cycles with a resistance change of less than 3% (Figure 2e). As shown in Figure 2f, the bicontinuous film showed the lowest electrode-skin impedances in the frequency range of 1–10^4 Hz in the comparison with typical flexible electrode material (e.g., Ag-Ga-TPU, PEDOT: PSS) and the impedance remained unchanged in one week (Figure 2g). Compared with other electrode materials,[3,11,22,24–26,30,31] the bicontinuous film exhibited higher electrical conductivity and lower impedance on the skin (Figure 2h), which is advantageous for fabricating high-sensitivity surface electrodes.

2.3. Electrophysiological Signals Monitoring

The obtained non-cytotoxic bicontinuous film (Figure S15, Supporting Information) adhered to the skin as a surface electrode to detect ECG of the rat model of myocardial infarction. The bicontinuous film electrodes monitored the characteristic peak of myocardial infarction at an earlier stage than commercial electrodes (Ag/AgCl) (**Figure 3a**; Figure S16, Supporting Information), and relevant pathological sections also confirmed the result (Figure S17, Supporting Information). The bicontinuous film electrodes exhibited ≈60% higher characteristic amplitudes compared with commercial electrodes for ECG signals under various conditions including ST elevation, T towering, and P towering (Figure 3b). To further evaluate the ECG stability of different states, the bicontinuous film electrodes were adhered to the chest (Figure 3c). The stability was assessed using the reciprocal of the baseline deviation between the T and P waves (TP deviation^{-1}), with a high TP deviation^{-1} indicating high stability. The TP deviation^{-1} of the commercial electrodes decreased significantly compared with the bicontinuous film electrodes as the oscillation frequency increased (Figure 3d). Moreover, the bicontinuous film electrodes were also capable of detecting higher R peaks of ECG signals on both dry and wet skin (Figure S18, Supporting Information).

The bicontinuous film electrodes were then applied to monitor EMG signals. The electrodes were adhered to the leg muscle of the volunteer, the two characteristic amplitudes were recorded during a one-time jump and the amplitude values were almost consistent (Figure 3e). After continuous jumping for 1000 cycles, no leakage of the liquid metal was observed, and the mass of the electrode remained unchanged (Figure S19, Supporting Information). The bicontinuous film electrodes were also used to detect EMG signals from a finger in flexion or extension (Figure 3f,g). Next, EMG signals from the volunteer's hand were

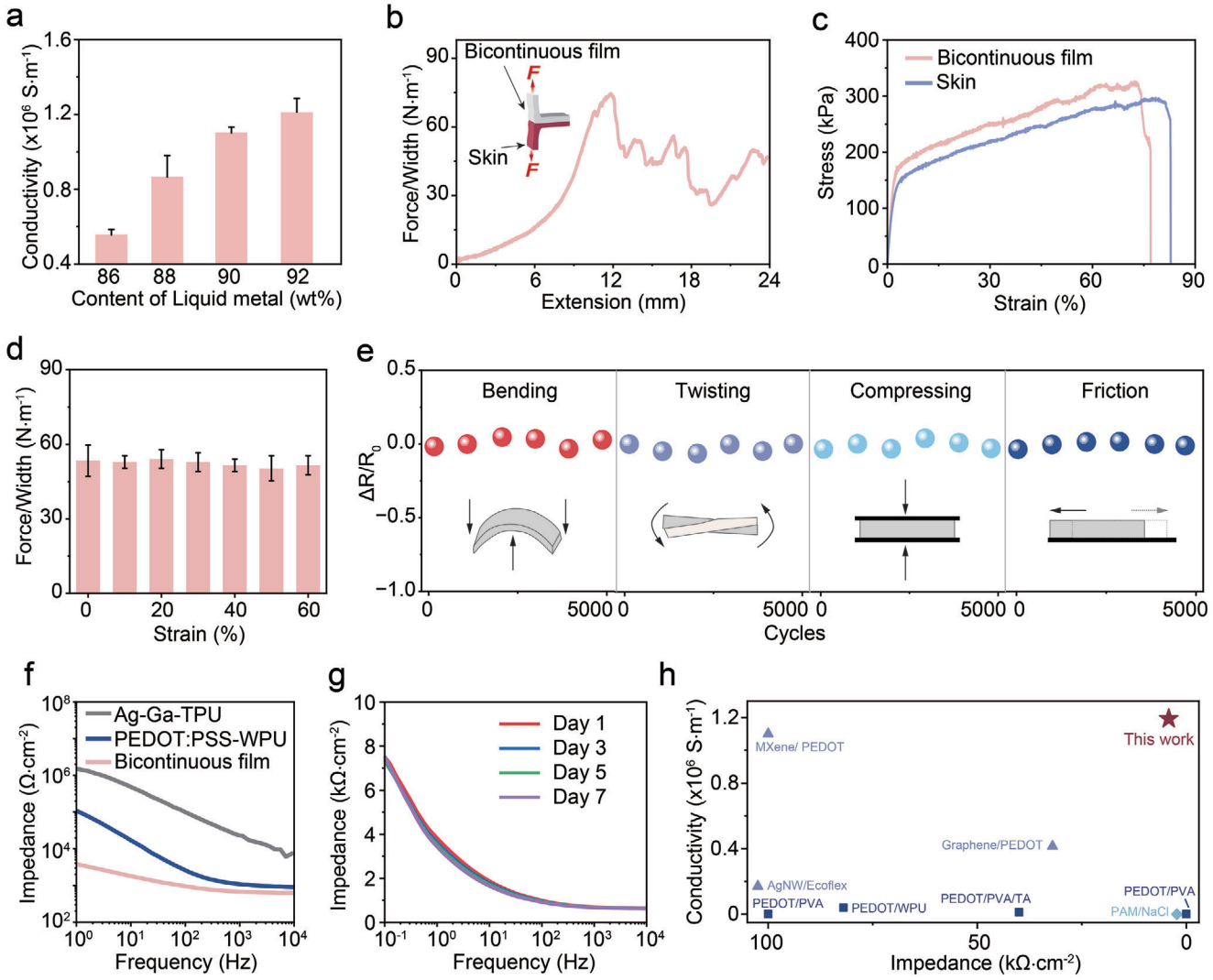

Figure 2. Electrical and mechanical properties of the bicontinuous film. a) Electrical conductivities of samples prepared with various mass fractions of liquid metal. All data are expressed as mean ± SD. Error bars, $n = 3$. b) Adhesion curves of bicontinuous film with 180° peeling test. c) Stress–strain curves of bicontinuous film and porcine skin. d) Representative adhesion curves of the bicontinuous film under different strains. All data are expressed as mean ± SD. Error bars, $n = 3$. e) $\Delta R/R_0$ response of bicontinuous film after bending, twisting, compressing, and friction each for 5000 cycles. f) Comparison of electrode-skin impedance among Ag-Ga-thermoplastic polyurethanes (TPU) electrodes, Poly(3,4-ethylenedioxythiophene) polystyrene sulfonate (PEDOT:PSS)-waterborne polyurethane (WPU) electrodes, and bicontinuous film. g) The stable impedance magnitude of bicontinuous film for one week in simulated sweat. h) The comparison of impedance on skin and conductivity of bicontinuous film with the reported surface electrode.

monitored under varying gripping forces. For large force changes (Δ = 10 N), the bicontinuous film electrodes demonstrated a higher signal-to-noise ratio (SNR) compared to the commercial Ag/AgCl electrodes (Figure S20, Supporting Information). For minor force changes (Δ = 1 N), the commercial electrodes exhibited irregular responses, whereas the bicontinuous film electrodes accurately reflected force changes with a sensitivity of 20 μV N^{-1} (Figure 3h,i; Figure S21, Supporting Information). Compared with other surface electrodes reported,[26,32–35] the bicontinuous film electrodes showed unexpected sensitivity, which was ≈400% higher than the highest performance reported to date (Figure 3j), and maintained the sensitivity above 90% even after multiple cycles of the attach/detach (Figure S22, Supporting Information).

2.4. Application of the Bicontinuous Film Electrodes

The highly sensitive bicontinuous film electrodes were also capable of accurately sensing and discriminating different materials based on slight electromyographic differences when fingers touch different materials. It is important to note that due to the similarity in tactile properties of different materials (such as elasticity, hardness, and friction coefficient), it is difficult for the previously reported electrodes to achieve this application. As shown in **Figures** 4a and S23 (Supporting Information), the bicontinuous film electrodes were attached to the surface of the arm, and the finger touched different material surfaces, with the EMG signals being monitored and collected in real-time. To ensure the consistency of finger pressure on the materials in each

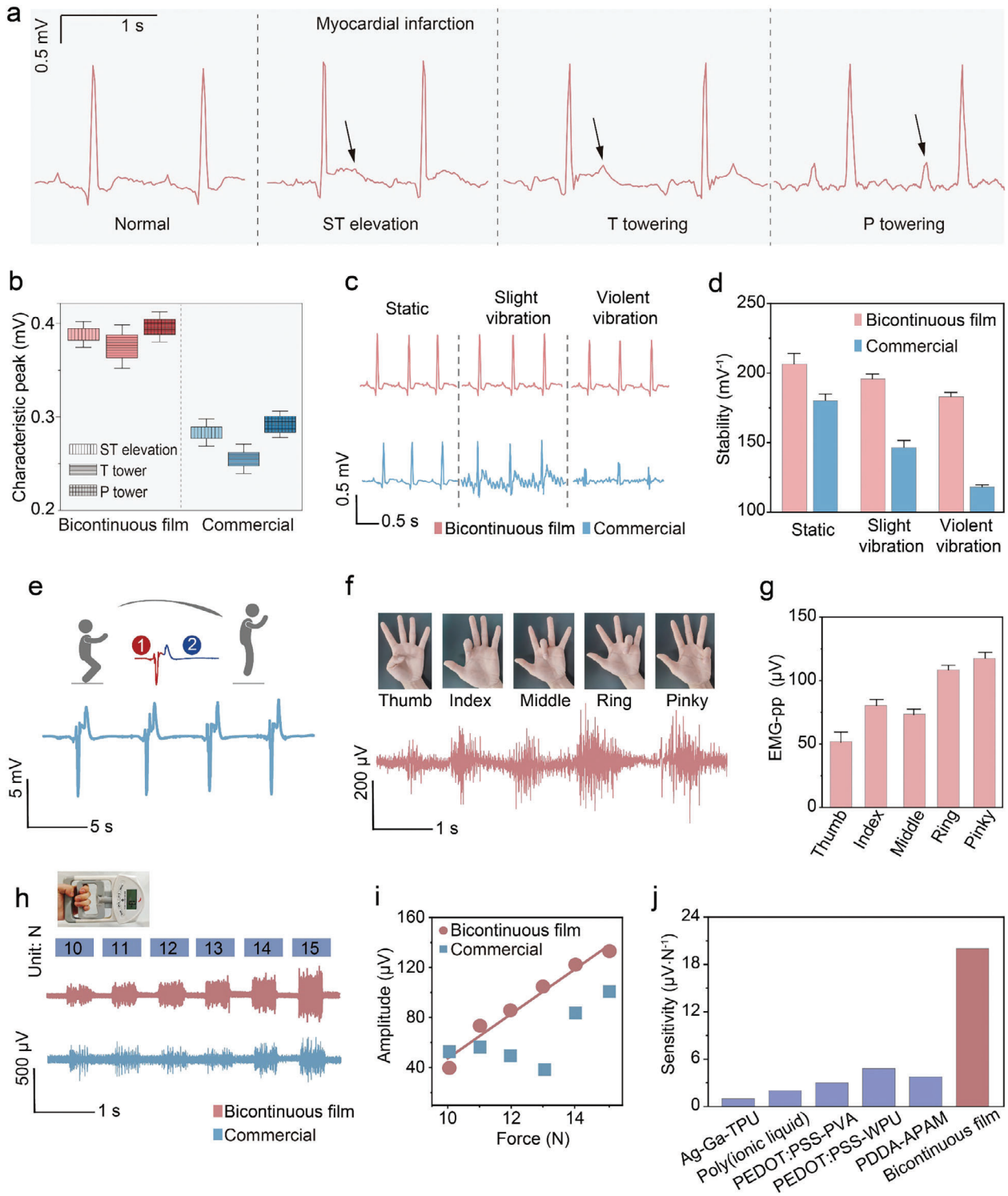

Figure 3. ECG and EMG detection using bicontinuous film electrodes. a) ECG signals showing the characteristic peak of different physiological status in the myocardial infarction. b) Comparison of values of characteristic peak obtained by bicontinuous film electrodes and commercial Ag/AgCl electrodes. All data are expressed as mean ± SD. Error bars, $n = 3$. c) ECG testing on the skin under motion induced by an electrical vibrator, including static, slight (vibration frequency ≈0.2 Hz), and violent (vibration frequency ≈2 Hz) state. d) Signal stability between bicontinuous film and commercial electrodes in three states. All data are expressed as mean ± SD. Error bars, $n = 3$. e) EMG signals detected by bicontinuous film electrodes in the process of the body jumping and f) the flexion/extension of different fingers. g) EMG signal intensities detected by bicontinuous film electrodes. All data are expressed as mean ± SD. Error bars, $n = 3$. h) Comparison of EMG signals by using bicontinuous film electrodes and commercial electrodes in different grip strength. i) The relationship between EMG-PP and grip strength. j) A critical comparison between this work and other reported literature in terms of the sensitivity of surface electrodes.

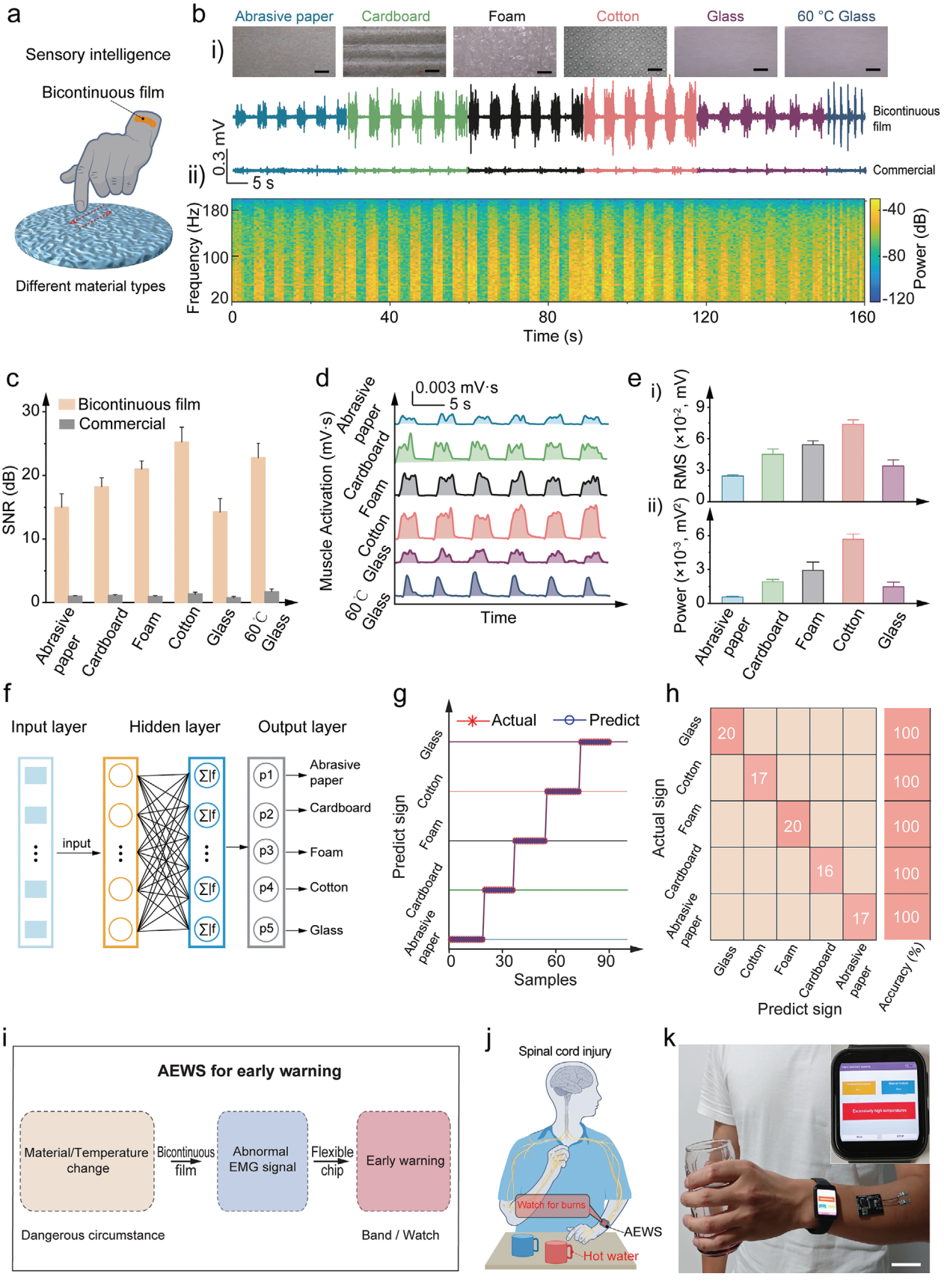

experiment, the fingers remained stationary during the testing process while the materials underwent relative periodic motion (Figure S24, Supporting Information). The pressure applied by the fingers to different materials was visualized through readings from an electronic scale and maintained at 10 ± 1 g. Due to the different stimulation caused by different material surfaces to the finger, the EMG signals generated varied, including abrasive paper, cardboard, foam, cotton, glass, and glass heated to 60 °C (Figure 4b; Figure S25, Supporting Information). Compared with commercial electrodes, the bicontinuous film electrodes demonstrated higher amplitude and excellent repeatability. Furthermore, the SNR of bicontinuous film electrodes was almost 10 times higher than that of commercial electrodes (Figure 4c). Accurate and reliable EMG signal monitoring was the prerequisite for material recognition.

Subsequently, the EMG signals needed to be processed with the aid of machine learning algorithms for material recognition. The corresponding algorithms developed included signal processing algorithms, position segmentation algorithms, feature parameter extraction procedures, and neural network classification algorithms. In terms of signal decoding, the collected signals were first filtered and denoised, and outliers were removed through signal processing algorithms to improve signal quality. Then, since EMG was spontaneously generated during active human movement and lacks temporal regularity, it was necessary to identify and localize the EMG signals of the material through a position segmentation algorithm. Next, feature parameter extraction procedures used the fast Fourier transform to extract feature values from these EMG signals in both the time and frequency domains. Due to the significant differences in EMG signals when touching different materials, 9 characteristic parameters were used. These parameters included muscle activation (Figure 4d), root mean square (RMS), power (Figure 4e), maximum power, maximum slope, standard error, minimum slope, maximum, and minimum (Figure S26, Supporting Information) for material recognition. Next, the extracted characteristic parameters of EMG signals were inputted into an artificial neural network (ANN), which was then used for model training and data mining. The ANN consisted of 9 input layers, 3 hidden layers, and 5 output layers (Figure 4f). After 400 training epochs, the accuracy and loss rate of the ANN model gradually stabilized (Figure S27, Supporting Information). Furthermore, through deep learning, the recognition of five material types in the test set achieved an accuracy of 100% (Figure 4g,h). In conclusion, the bicontinuous film electrodes combined with machine learning algorithms had promising applications in material recognition.

An AI-enabled active early warning system (AEWS) was further constructed using the bicontinuous film electrodes. Specifically, the workflow diagram of the wearable system for active early warning is shown in Figure 4i. The electromyographic signals collected in real-time from the bicontinuous film electrodes were converted into digital signals using a self-designed flexible chip and were wirelessly transmitted to a server. The received signals were analyzed with the assistance of machine learning to identify changes in materials or abnormal temperatures. When a dangerous or abnormal situation occurred, the system promptly alerted the patient through a smartwatch to avoid risk. For example, for individuals with spinal cord injuries who could move their fingers normally but whose related central nervous system could not perceive external stimuli, AEWS provided real-time warnings of dangerous contact (Figure 4j). As a proof-of-concept, when the volunteer simulated a spinal cord injury patient and picked up a cup of hot water, the AEWS promptly alerted the volunteer to the material/temperature-related danger through the smartwatch (Figure 4k). The warning stopped when the volunteer put down the hot water cup.

3. Conclusion

In conclusion, we have developed a highly sensitive surface electrode by designing a bicontinuous liquid metal/polymer film material that combines fast electron transport, enhancing skin adhesion, and conformal contact with the skin. The resulting electrode achieved a sensitivity of 20 μV N^{-1}, an increase of ≈400% over the highest performance reported to date. The electrode is capable of detecting electrocardiographic abnormalities at an earlier stage and can be further combined with machine learning algorithms to prevent hazardous situations for individuals with tactile impairments. This work may open up a new direction in developing high-performance surface electrodes and inspire more intelligent wearable applications.

Supporting Information

Supporting Information is available from the Wiley Online Library or from the author.

Acknowledgements

J.L. and Q.L. contributed equally to this work. The animal experiments were operated according to the Animal Experimentation Committee of Nanjing University of Chinese Medicine (approval number 202408A035). This work was financially supported by the National Natural Science Foundation of China (52422310 and 22175086), the Natural Science Foundation of Jiangsu Province (BK20240169), the Program for Innovative Talents and Entrepreneurs in Jiangsu (JSSCTD202138).

Figure 4. Application of bicontinuous film electrodes. a) Schematic illustration of finger touch on different material surfaces. b) EMG signals (i) and spectrograms (ii) recorded by bicontinuous film and commercial electrodes (Ag/AgCl), respectively. For abrasive paper, cardboard, foam, cotton, and glass, the volunteer was asked to retract for 5 s each time. For the 60 °C glass, due to the risk of skin burns from prolonged high-temperature contact, the volunteer was asked to retract for 2 s each time. c) Comparison of SNR values of the EMG signals obtained by bicontinuous film and commercial electrodes (Ag/AgCl). $n = 6$. d) The muscle activity obtained by EMG signal processing. $n = 6$. e) Statistical analysis of EMG signals recorded by bicontinuous film electrodes for different material types, which the RMS values (i) and power of EMG signals (ii) captured ($n = 6$). f) The ANN for the training and recognition simulation of 5 material types. g) Comparison of testing set prediction results. h) Confusion matrix of the test set for ANN model. i) Block diagram shows how the bicontinuous film electrodes works in AEWS. j) Schematic illustration of AEWS giving a warning when a person with spinal cord damage touches hot water. k) Photograph of a volunteer wearing the AEWS. The inset is a Photograph of the watch display interface. Scale bars, 3 cm.

Conflict of Interest

The authors declare no conflict of interest.

Data Availability Statement

The data that support the findings of this study are available from the corresponding author upon reasonable request.

Keywords

conductive film, electrophysiological signal, high sensitivity, polymer electrode

Received: November 3, 2024
Revised: November 19, 2024
Published online:

[1] G. Yang, K. Zhu, W. Guo, D. Wu, X. Quan, X. Huang, S. Liu, Y. Li, H. Fang, Y. Qiu, Q. Zheng, M. Zhu, J. Huang, Z. Zeng, Z. Yin, H. Wu, *Adv. Funct. Mater.* **2022**, *32*, 2200457.
[2] Q. Tian, H. Zhao, X. Wang, Y. Jiang, M. Zhu, H. Yelemulati, R. Xie, Q. Li, R. Su, Z. Cao, N. Jiang, J. Huang, G. Li, S. Chen, X. Chen, Z. Liu, *Adv. Mater.* **2023**, *35*, 2211236.
[3] H. Wang, Q. Ding, Y. Luo, Z. Wu, J. Yu, H. Chen, Y. Zhou, H. Zhang, K. Tao, X. Chen, J. Fu, J. Wu, *Adv. Mater.* **2024**, *36*, 2309868.
[4] Z. Zhao, H. Zhu, X. Li, L. Sun, F. He, J. E. Chung, D. F. Liu, L. Frank, L. Luan, C. Xie, *Nat. Biomed. Eng.* **2023**, *7*, 520.
[5] W. Zhou, Y. Jiang, Q. Xu, L. Chen, H. Qiao, Y.-X. Wang, J.-C. Lai, D. Zhong, Y. Zhang, W. Li, Y. Du, X. Wang, J. Lei, G. Dong, X. Guan, S. Ma, P. Kang, L. Yuan, M. Zhang, J. B. H. Tok, D. Li, Z. Bao, W. Jia, *Nat. Biomed. Eng.* **2023**, *7*, 1270.
[6] D. Farina, I. Vujaklija, M. Sartori, T. Kapelner, F. Negro, N. Jiang, K. Bergmeister, A. Andalib, J. Principe, O. C. Aszmann, *Nat. Biomed. Eng.* **2017**, *1*, 0025.
[7] G. Shafiei, B. D. Fulcher, B. Voytek, T. D. Satterthwaite, S. Baillet, B. Misic, *Nat. Commun.* **2023**, *14*, 6000.
[8] B. Coughlin, W. Muñoz, Y. Kfir, M. J. Young, D. Meszéna, M. Jamali, I. Caprara, R. Hardstone, A. Khanna, M. L. Mustroph, E. M. Trautmann, C. Windolf, E. Varol, D. J. Soper, S. D. Stavisky, M. Welkenhuysen, B. Dutta, K. V. Shenoy, L. R. Hochberg, R. M. Richardson, Z. M. Williams, S. S. Cash, A. C. Paulk, *Nat. Protoc.* **2023**, *18*, 2927.
[9] X. Zhang, G. Zhu, M. Chen, X. Chen, X. Chen, P. Zhou, *IEEE Trans. Neural Syst. Rehabil. Eng.* **2020**, *28*, 3148.
[10] H. Wu, G. Yang, K. Zhu, S. Liu, W. Guo, Z. Jiang, Z. Li, *Adv. Sci.* **2021**, *8*, 2001938.
[11] J. H. Shin, J. Y. Choi, K. June, H. Choi, T.-i. Kim, *Adv. Mater.* **2024**, *36*, 2313157.
[12] K. C. Siontis, P. A. Noseworthy, Z. I. Attia, P. A. Friedman, *Nat. Rev. Cardiol.* **2021**, *18*, 465.
[13] Q. Han, C. Zhang, T. Guo, Y. Tian, W. Song, J. Lei, Q. Li, A. Wang, M. Zhang, S. Bai, X. Yan, *Adv. Mater.* **2023**, *35*, 2209606.
[14] B. Vogel, B. E. Claessen, S. V. Arnold, D. Chan, D. J. Cohen, E. Giannitsis, C. M. Gibson, S. Goto, H. A. Katus, M. Kerneis, T. Kimura, V. Kunadian, D. S. Pinto, H. Shiomi, J. A. Spertus, P. G. Steg, R. Mehran, *Nat. Rev. Dis. Primers* **2019**, *5*, 39.
[15] K. Bayoumy, M. Gaber, A. Elshafeey, O. Mhaimeed, E. H. Dineen, F. A. Marvel, S. S. Martin, E. D. Muse, M. P. Turakhia, K. G. Tarakji, M. B. Elshazly, *Nat. Rev. Cardiol.* **2021**, *18*, 581.
[16] H. Yuk, J. Wu, X. Zhao, *Nat. Rev. Mater.* **2022**, *7*, 935.
[17] H. Yuk, B. Lu, X. Zhao, *Chem. Soc. Rev.* **2019**, *48*, 1642.
[18] S. F. Cogan, *Annu. Rev. Biomed. Eng.* **2008**, *10*, 275.
[19] M. Lu, C. Huang, Z. Xu, Y. Yuan, M. Wang, M. Xiao, L. Zhang, P. Wan, *Adv. Funct. Mater.* **2023**, *33*, 2306591.
[20] L.-W. Lo, J. Zhao, K. Aono, W. Li, Z. Wen, S. Pizzella, Y. Wang, S. Chakrabartty, C. Wang, *ACS Nano* **2022**, *16*, 11792.
[21] E. K. Lee, M. K. Kim, C. H. Lee, *Annu. Rev. Biomed. Eng.* **2019**, *21*, 299.
[22] S. Yang, J. Cheng, J. Shang, C. Hang, J. Qi, L. Zhong, Q. Rao, L. He, C. Liu, L. Ding, M. Zhang, S. Chakrabarty, X. Jiang, *Nat. Commun.* **2023**, *14*, 6494.
[23] S. Kabiri Ameri, R. Ho, H. Jang, L. Tao, Y. Wang, L. Wang, D. M. Schnyer, D. Akinwande, N. Lu, *ACS Nano* **2017**, *11*, 7634.
[24] D. Song, X. Li, M. Jang, Y. Lee, Y. Zhai, W. Hu, H. Yan, S. Zhang, L. Chen, C. Lu, K. Kim, N. Liu, *Adv. Mater.* **2023**, *35*, 2304956.
[25] Y. Zhao, S. Zhang, T. Yu, Y. Zhang, G. Ye, H. Cui, C. He, W. Jiang, Y. Zhai, C. Lu, X. Gu, N. Liu, *Nat. Commun.* **2021**, *12*, 4880.
[26] L. Zhang, K. S. Kumar, H. He, C. J. Cai, X. He, H. Gao, S. Yue, C. Li, R. C.-S. Seet, H. Ren, J. Ouyang, *Nat. Commun.* **2020**, *11*, 4683.
[27] J. Cutinho, B. S. Chang, S. Oyola-Reynoso, J. Chen, S. S. Akhter, I. D. Tevis, N. J. Bello, A. Martin, M. C. Foster, M. M. Thuo, *ACS Nano* **2018**, *12*, 4744.
[28] S. Liu, S. N. Reed, M. J. Higgins, M. S. Titus, R. Kramer-Bottiglio, *Nanoscale* **2019**, *11*, 17615.
[29] A. Kihara, *Prog. Lipid Res.* **2016**, *63*, 50.
[30] J. Cao, X. Yang, J. Rao, A. Mitriashkin, X. Fan, R. Chen, H. Cheng, X. Wang, J. Goh, H. L. Leo, J. Ouyang, *ACS Appl. Mater. Interfaces.* **2022**, *14*, 39159.
[31] S. Yao, W. Zhou, R. Hinson, P. Dong, S. Wu, J. Ives, X. Hu, H. Huang, Y. Zhu, *Adv. Mater. Technol.* **2022**, *7*, 2101637.
[32] W. Wang, H. Song, Z. Lu, Q. Zeng, Q. Wang, C. Ma, H. Jin, J. Qi, T. Wu, S. Gao, M. Zhu, D. Lu, J. Huang, Y. Yan, *Adv. Mater. Interfaces.* **2022**, *9*, 2201367.
[33] M. Reis Carneiro, C. Majidi, M. Tavakoli, *Adv. Funct. Mater.* **2022**, *32*, 2205956.
[34] S. Zheng, W. Li, Y. Ren, Z. Liu, X. Zou, Y. Hu, J. Guo, Z. Sun, F. Yan, *Adv. Mater.* **2022**, *34*, 2106570.
[35] P. Tan, H. Wang, F. Xiao, X. Lu, W. Shang, X. Deng, H. Song, Z. Xu, J. Cao, T. Gan, B. Wang, X. Zhou, *Nat. Commun.* **2022**, *13*, 358.